PHAS0097 PHYSICS PROJECT

Design of a Wien filter for use with Ionic Liquid Ion Sources

by

Usama Ahmed

Supervised by Carla S. Perez Martinez

Natural Sciences: Condensed Matter Physics and Inorganic & Materials Chemistry

UCL DEPARTMENT OF PHYSICS & ASTROMOMY

Submission of coursework for Physics and Astronomy course PHAS0097/PHAS0048
2020/21

Please sign, date and return this form with your coursework by the specified deadline.

DECLARATION OF OWNERSHIP

I confirm that I have read and understood the guidelines on plagiarism, that I understand the meaning of plagiarism and that I may be penalised for submitting work that has been plagiarised.

I confirm that all work will also be submitted electronically and that this can be checked using the JISC detection service, Turnitin®.

I declare that all material presented in the accompanying work is entirely my own work except where explicitly and individually indicated and that all sources used in its preparation and all quotations are clearly cited.

Should this statement prove to be untrue, I recognise the right of the Board of Examiners to recommend what action should be taken in line with UCL's regulations.

Signed UsamaAhmed

PrintName Usama Ahmed

Dated 26/04/2021

Title	Date Received	Examiner	Examiner's Signature	Mark

Abstract

Ionic liquid ion sources provide purely ionic beams of positive and negative ions via field evaporation from room-temperature molten liquid salts and offer better irradiation characteristics than current technologies. Emitted ions can undergo fragmentation resulting in widened energy distributions and lower resolutions which is problematic for material irradiation. A velocity selector, or Wien Filter, is necessary to isolate desirable highly energetic monomer ions. We propose and test a design for a Wien filter using COMSOL Multiphysics. Field qualities are investigated and particle trajectories and escape percentages are evaluated for ionic liquid 1-Ethyl-3-methylimidazolium tetrafluoroborate ($EMI - BF_4$). The filter is found to reduce desirable monomer count by 88.8 % for a conical beam while removing some but not all undesirable ionic species.

Contents

1 Introduction

Ionic Liquid Ion Sources (ILIS) make use of room-temperature molten liquid salts, composed of non-solvent mixtures of complex organic and inorganic ions. A typical ionic liquid is 1-Ethyl-3-methylimidazolium tetrafluoroborate ($\mathrm{EMI-BF_4}$), illustrated in figure 1.

ILIS utilises a beam of ions, either passed through a capillary, or more recently, used to externally wet a needle [2] and are capable of emitting both positive and negative ions, unlike existing technologies like liquid metal ion sources (LMIS) which only emit positive ions. If a sufficiently large potential difference is applied between the needle tip and a grounded aperture (extractor), typically placed 1 mm downstream [3], the electric field generated at the emitter tip overcomes the surface tension of the liquid which evolves into a sharpened meniscus. Direct ion emission can then result where the ions are accelerated in the acceleration region (AR) [4] and ejected into the field free region (FFR). An illustration of an ILIS emitter is shown in figure 2. This beam can then be filtered, focused and directed towards a substrate requiring treatment.

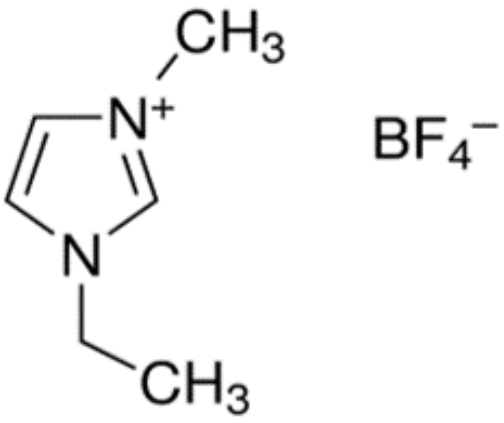

Figure 1: Illustration of a prototypical ionic liquid 1-Ethyl-3-methylimidazolium tetrafluoroborate ($\mathrm{EMI-BF_4}$) used in ILIS. Figure Adapted from reference [1].

Emission results in some metastable clusters that can break up and undergo fragmentation, both in the AR and the FFR, and result in smaller species [5]. This fragmentation introduces unwanted species and widens the energy distribution of the final beam. This is problematic because substrate irradiation demands control over the exact species of ion, especially for focused ion beams (FIB) that require paraxial, mono-energetic, homogeneous beams with narrow energy distributions and adequate resolution. FIB is a technique particularly used in the semiconductor and materials science industry that focuses a beam of ions, using dedicated optics, for material analysis, etching and lithography [6].

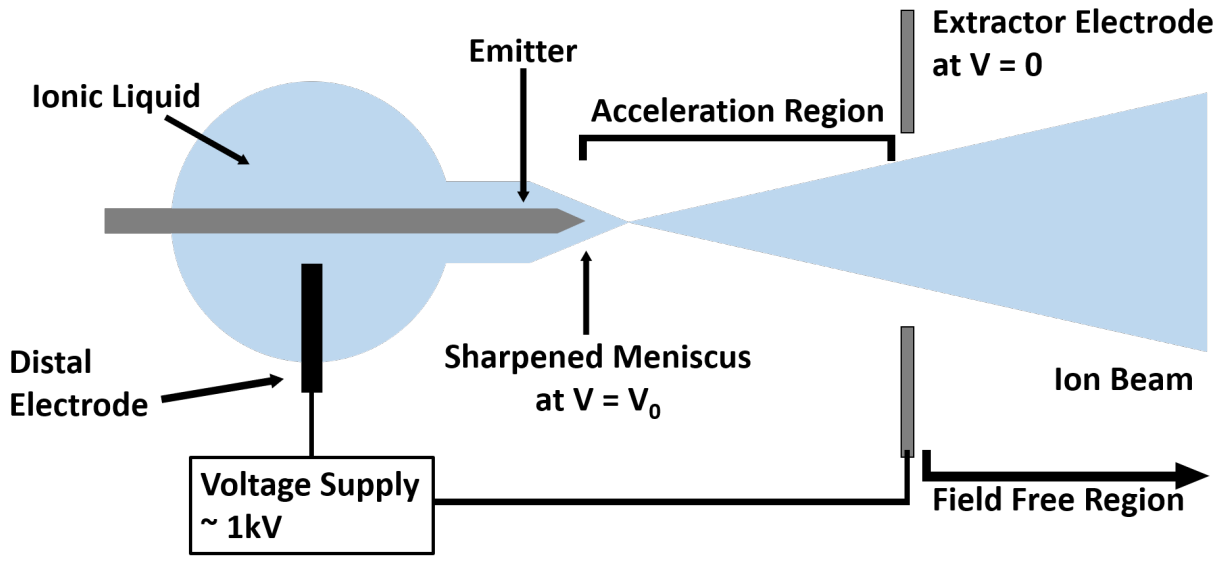

Figure 2: Schematic illustration of an ILIS emitter where an ionic liquid externally wets an emitter needle, typically tungsten. Ions are evaporated at the meniscus at voltage V_0 and then accelerated in the AR to the extractor electrode at voltage $V = 0$. Fragmentation can occur both in the AR and the FFR. A distal electrode applies an electric potential V_0 to the ILIS while avoiding contact with the electrode to minimise unwanted electrochemical reactions.

A Wien filter, illustrated in figure 3 can be used to separate ions based on their velocity. Also known as an ExB filter, a Wien filter is a velocity selector that utilises uniform perpendicular electric (E) and magnetic (B) fields to deflect charged particles, letting through those with velocity $v = \frac{E}{B}$ undeflected, where the forces from the electric and magnetic fields, F_E and F_B, equal each other. Herein, we aim to design a Wien filter suitable for work in a practical laboratory making use of an ILIS column. We start by summarising key historical developments in section 2 and providing motivation for the current project by exploring the use and potential of ILIS in material irradiation in section 3. We then follow key studies investigating the nature of an ILIS beam in section 4. We proceed by deriving a mathematical model of particle trajectories through a theoretical Wien filter, in section 5 by first considering how fragmentation results in the make-up of our beam and then, deriving and analytically solving a set of differential equations that describe the displacements and

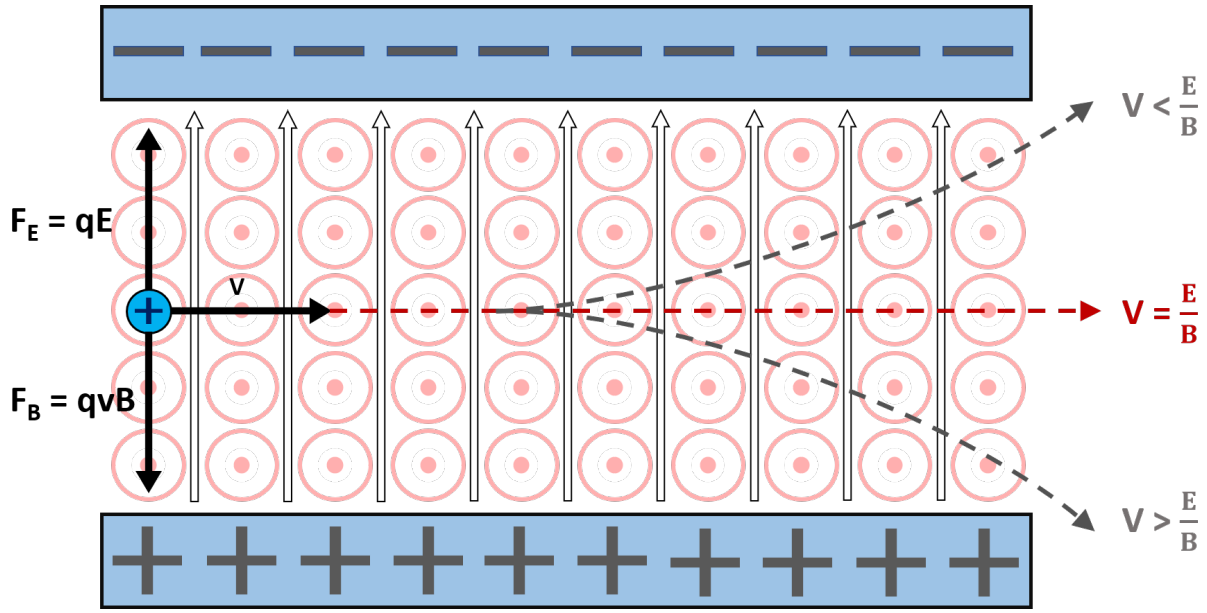

Figure 3: Schematic illustration of a Wien filter that uses a uniform electric (white arrows) field, going up the page, and magnetic (pink circles) field, coming out of the page, and the trajectory of a positive particle with velocity v where the particle passes straight through if $F_{\mathrm{E}} = F_{\mathrm{B}}$.

velocities through the filter. MATLAB is used to solve this model and obtain estimates of filter parameters like length and electric and magnetic field strengths required in section 5.1. Finally, section 6.1 proposes a Wien filter utilising permanent magnets and electrostatic deflectors, designed and evaluated in COMSOL Multiphysics. COMSOL Multiphysics is a general purpose simulation software that uses advanced numerical methods to solve physics-based models and simulations, that is used widely in industry and academia. The quality of the eletric and magentic field studies is investigated in section 6.2. The efficacy of the filter is tested by calculating ion trajectories of various ionic species in section 6.3. A discussion of errors is presented in section 6.4. Finally, a brief summary of findings and avenues for further work are suggested in section 7.

2 Historical Context

In 2003, Romero et al [7] first demonstrated emission in the pure ionic regime (PIR) using $EMI-BF_4$ and a tungsten emitter. Later studies by Lozano and Martínez-Sanchéz [8, 9] showed the beam to be composed of a mix of $(EMI-BF_4)EMI^+$ and EMI^+ in positive emission and $(EMI-BF_4)EMI^-$ and BF_4^- in negative emission. Operation in single polarity, direct current (DC) mode was found to leave counterions behind at the tip. These caused unwanted electrochemical reactions on the needle surface, causing rapid deterioration in beam quality with no appreciable current in 3-4 hours even with an increasing voltage [10]. This deterioration of the beam occurs due to the formation of a charge-double layer (CDL) at the emitter-liquid interface, much like a capacitor. Upon current extraction i.e. emission of ions, the generation of a large electric field at this interface can pass the electrochemical window for the liquid, triggering reactions at the interface. Lozano and Martínez-Sanchéz [9] found that an alternating current (AC) voltage, with a frequency of 1 Hz was sufficient to eliminate these unwanted electrochemical reactions and obtain a long-lasting PIR emission. The AC voltage ensures that the electric field generated at the CDL does not exceed the electrochemical window of the ionic liquid before the polarity switches again. Later, Brikner and Lozano [11] showed that using an upstream distal electrode to apply an indirect (at a distance) potential, further mitigates electrochemical degradation of ILIS emitter tips operating in DC mode. Subsequently, current studies with ILIS columns use AC voltages and an externally wetted emitter; most commonly Tungsten but others like Carbon Xerogel [6] have been explored.

3 Use of ILIS in Material Irradiation

Ion beams are widely used in the semiconductor, materials processing and surface analytical industries, for etching (material removal), lithography (material deposition) and various nano- and micro-fabrication processes [6]. Currently, LMIS are the most widely used ion source for FIB applications. Metals with low surface tensions and melting points, like Ga, In, Bu, Al, Sn, Cs, Cu and Au, are typically used [6]. Metals can be alloyed to produce

liquid metal alloy ion beams that allow one to tailor the beam to suit the application. The ionic species used greatly affects material irradiation properties and Wien filters have already been employed in liquid metal alloy columns to select only the desired ionic species [12].

LMIS has key disadvantages: The metal source exclusively produces positive ions limited to a mass/ charge (m/q) of less than 200 Dalton [7], leading to undesirable substrate charging, requiring remediation with external electron flooding systems. They are also restricted in chemical composition and are largely unreactive on their own. The metal ions can only remove material mechanically and thus require the use of expensive precursor gases [6] to achieve accelerated material removal.

ILIS are a promising alternative to LMIS technology. They produce very diverse ion beams, of both positive and negative ions, in terms of their masses, chemical reactivity, and composition due to the hundreds of available ionic liquids [6]. They have extraordinarily low surface tensions requiring smaller voltages than LMIS systems to trigger field evaporation. They have low melting points that minimize any reaction between the liquid and needle, thereby extending beam life and do not require chemical precursors for accelerated etching. A key of advantage of ILIS with respect to LMIS is their enhanced sputtering yields. Sputtering yield is defined as the ratio of the number of atoms removed from the sample to the number of incident ions. Sputtering yields using $\mathrm{EMI-BF_4}$, in positive emission, with irradiation energies between 2-7 keV on silicon, gold and gallium are found to be higher than using traditional Ga beams at much higher irradiation energies [13]. Similar is found by Yoshida et al, for a Silicon target [14], where ionic liquid 1-ethyl-3-methylimidazolium bis(trifluoromethylsulfonyl)imide (EMIM-TFSI) showcases a sputtering yield of 11.9 atoms per ion, at acceleration votlages of 5 kV, a 5.4-fold increase in sputtering yield compared to Ga, which is accelerated at a higher 30 kV and produces sputtering yields of 2.2 atoms. As the molecules arrive on the substrate, the kinetic energy of these ions causes dislocation of surface atoms from the target and breakage of chemical bonds in the incident ion. The resulting free radicals e.g. F^- react with the sputtered particles to create volatile species that aid material removal [15]. Substrates analysed post-sputtering via X-ray photoelectron spectroscopy (XPS) show a new chemical environment appearing with silicon substrates showing Si-C and Si-N bonds on the surface. [16].

The use of negative ions from ILIS avoids substrate charging and can lead to higher etching rates and sputtering yields with respect to LMIS [17]. Etching depths on silicon using DCA^- anions from a 1-ethyl-3-methylimidazolium dicyanamide ($EMIM - DCA$) beam are found to be two times higher than with $EMIM^+$ at the same energy [18], despite the molecular weight of DCA^- being lower than $EMIM^+$. Similar is found by Xu et al [4], who found increased etching rates on Si and SiO_2 substrates using $EMI - BF_4$ in negative emission. The increase in sputtering yield is attributed to higher chemical reactivity of ionic species in ILIS with respect to their LMIS counterparts and the lack of substrate charging with negative ions [4].

4 Beam Characterisation

Given an ionic liquid AB, with A^+ cation and B^- anion, at the point of emission the beam from an ILIS in positive emission mode consists of oligomer ions of the type $(AB)_{\mathrm{k}}A^+$, most commonly monomers ($k = 0$, A^+), dimers ($k = 1$, $(AB)A^+$) and trimers (k = 2, $(AB)_2A^+$); although higher order species may be found in small numbers [5]. Oligomer ions with $k \geq 1$ are prone to fragmentation, either in the AR between the emission tip and the extractor and/ or the FFR beyond the extractor, breaking up into smaller units like monomers, neutrals and other oligomers. Thus, the composition of the final beam is different from that at the point of emission.

Perez-Martinez et al [19] have characterised the shape of an ILIS beam using EMI-BF4. Figure 4 shows that the beam is parabolic in shape, with a decaying intensity radially outwards.

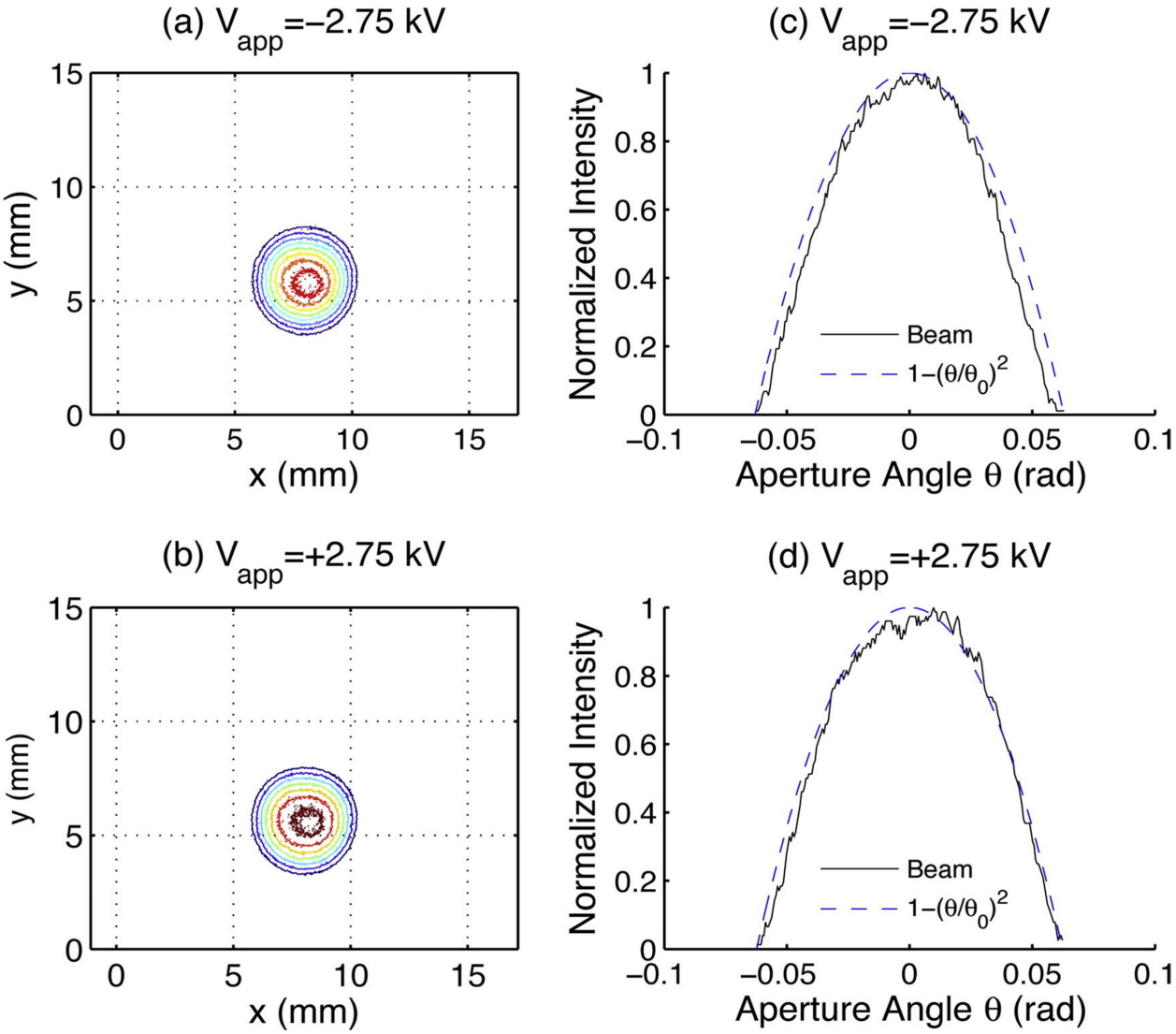

Figure 4: Contour plots of (a) positive and (b) negative ion beam profiles and cross-sections of (c) positive and (d) negative ion beams, compared a perfect parabola shown by the dotted line. Figure adapted from reference [19].

Miller et al [5] have found that 20% of the dimers, using (1-ethyl-3-methylimidazolium tris(pentafluoroethyl)trifluorophosphate) EMI-FAP, undergo fragmentation in the FFR with a source voltage of 809V, shown in figure 5. These results are corroborated by Fedkiw et al [20] who found a 1-butyl-3-methylimidazolium iodide (BMI-I) beam, in the negative emission mode, to contain significant fragmentation.

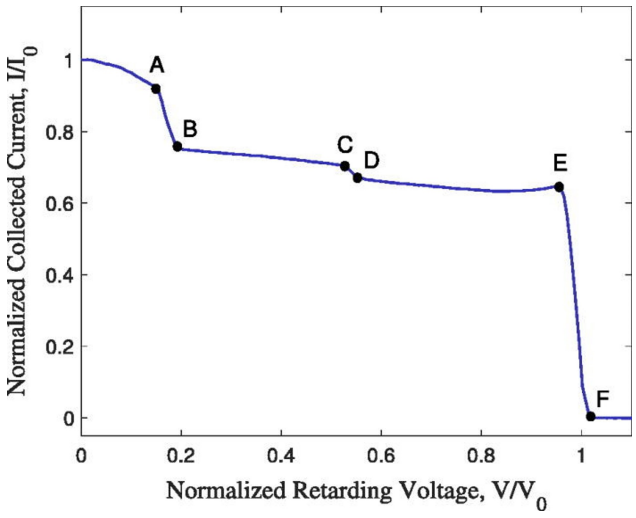

Figure 5: (Retarding potential analysis) RPA curve showing normalised current against retarding voltage for EMI − FAP externally wetting a Carbon xerogel emitter at an acceleration voltage of 809 V. Figure taken from [5].

Observing figure 5; the step between A and B indicates the fraction of dimers that dissociate in the FFR. The step between B and C corresponds to dimer dissociation within the AR. The step between C and D corresponds to trimer dissociation in the FFR. The step between D and E corresponds to dissociation of a variety of ion cluster species and the step between E and F indicates the fraction of ions with source potential energy [5]. The sharpness of the steps in figure 5 are illustrative of the narrow energy distributions of ILIS. Figure 6 shows the dimer dissociation rate in the FFR, for EMI-BF4, EMI-Im (1-ethyl-3-methylimidazolium bis(trifluoromethylsulfonyl)imide), EMI-FAP and BMI-I, in negative emission, plotted against molecular degrees of freedom [20]. With BMI-I as an exception, ion clusters composed of complex molecular ions, with higher degrees of freedom are found to dissociate at lower rates. In conclusion, ILIS beams offer small energy deviations from the applied voltage, while offering better etching performances and reactivities that can be tailored for a larger variety of applications, with milder operating conditions. Practically every ionic liquid measured can emit in the PIR [21], however, past ILIS experiments have always been done with mixed-ion beams without the use of Wien filters, which have been put to good use in LMIS beams. Research in Wien filters is necessary to give purely ionic homogenous, mono-energetic ILIS beams, suitable for high-throughput, high-resolution work.

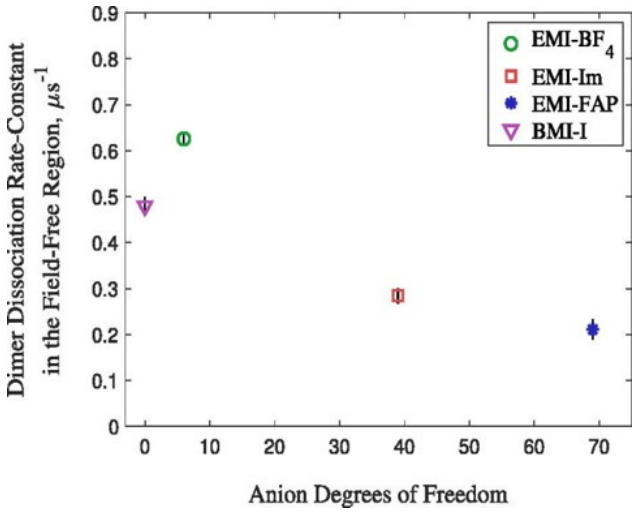

Figure 6: Dissociation rate against calculated degrees of freedom of $\mathrm{EMI}-\mathrm{BF}_4$, $\mathrm{EMI}-\mathrm{Im}$, $\mathrm{EMI}-\mathrm{FAP}$ and $\mathrm{BMI}-\mathrm{I}$. Figure adapted from [20].

5 Mathematical Model

Given an ionic liquid AB, let us define the masses of the cation A^+ and anion B^- as m_{A} and m_{B}, respectively. Respecting fragmentation, the final beam from such an ILIS emission consists of

- Direct emission (DE) monomers, that evaporated directly from the meniscus and that underwent full acceleration in the AR. The Wien filter seeks to isolate these monomers. These monomers have mass m_{A} and velocity $v_{\mathrm{DE},0}$
- Direct emission (DE) oligomers $(AB)_{\mathrm{k}}A^+$, of mass $m_{\mathrm{k}} = k(m_{\mathrm{A}}+m_{\mathrm{B}})+m_{\mathrm{A}}$ and velocity $v_{\mathrm{DE,k}}$ that underwent full acceleration in the AR.
- Monomers resulting from fragmentation in the FFR, henceforth referred to as FFR monomers. These have mass $\mathrm{m_A}$ and velocity $\mathrm{v_{DE,k}}$.
- Monomers resulting from fragmentation in the AR, henceforth referred to as AR monomers; these fragmented monomers have mass m_{A} and final velocity v_{b} that depends on where, in the AR, the fragmentation occurred.
- Neutrals $(AB)_{\mathrm{k}}$ resulting from fragmentation events

We aim to design a Wien filter that will isolate DE monomers while deflecting and trapping all other ionic species. Note that since neutral species are uncharged, they are not deflected in the Wien filter and additional deflectors downstream are necessary to remove these, therefore we restrict our analysis to charged ionic species only. Additionally, while an ILIS emitter can emit both in positive and negative emission modes, here for brevity, all analysis is done assuming positive emission although the physics is the same for negative emission. Furthermore, a large amount of oligomers in practical ILIS beams are dimers, with small amounts of trimers and tetramers [5]. A Wien filter that can successfully deflect and remove dimers will always deflect and remove larger, more massive hence slower higher order oligomers. Therefore, in this report we contain our analysis to dimers and smaller species only. Finally, we assume that dimer fragmentation strictly results in a monomer A^+ and a $(AB)_\mathrm{k}$ neutral, which is largely the case in practical beams [18].

We now proceed to derive a mathematical model that can analytically solve for ion trajectories in a Wien filter. We start by deriving expressions for the the velocities of the aforementioned ionic species. For an emitter at voltage V_0, the velocities $v_{\mathrm{DE},0}$ and $v_{\mathrm{DE,k}}$ can be derived by considering that a particle with charge q and mass m accelerated to an electric potential V_0 gains a kinetic energy $\frac{1}{2}mv^2$. Substituting monomer and oligomers masses m_A and m_k for m into the kinetic energy and solving for the resultant velocities we obtain

$$v_{\mathrm{DE},0} = \sqrt{\frac{2qV_0}{m_A}} \tag{1}$$

$$v_{\mathrm{DE,k}} = \sqrt{\frac{2qV_0}{m_\mathrm{k}}} \tag{2}$$

We now obtain an expression for the velocity v_b of AR monomers. Fragmentation in the AR can occur at any point between the meniscus, which is at potential V_0, and the extractor which is at ground; fragmentation in the FFR occurs at zero electric potential. We define v_a as the velocity of the oligomer immediately before fragmentation in the AR, when the oligomer has left the meniscus but is still undergoing acceleration. Note that this is also the velocity of the resulting monomer and neutral cluster immediately after break-up. If fragmentation occurs at a potential V_b, where $0 \leq V_\mathrm{b} \leq V_0$, conservation of energy gives us

$$\frac{1}{2}m_A v_\mathrm{b}^2 = \frac{1}{2}m_A v_\mathrm{a}^2 + qV_\mathrm{b} \tag{3}$$

The oligomer velocity before fragmentation, v_{a}, can be obtained by considering the kinetic energy of the oligomer at the point of break-up. Let $V_{\mathrm{b}} = \alpha V_0$ where $0 \leq \alpha \leq 1$. We then have that

$$v_{\mathrm{a}} = \sqrt{\frac{2qV_0(1-\alpha)}{m_{\mathrm{k}}}} \tag{4}$$

Substituting expression 4 into expression 3 and solving for AR monomer velocity v_{b} gives us

$$v_{\mathrm{b}} = \sqrt{\frac{2qV_0(m_A + \alpha(m_{\mathrm{k}} - m_A))}{m_A m_{\mathrm{k}}}} \tag{5}$$

Once the beam exits the aperture, it is received by the Wien filter. Expressions 1 and 5 give us the velocities at which DE monomers and AR monomers enter the Wien filter while expression 2 gives us the velocities at which DE oligomers and FFR monomers enter the filter.

In order to inform filter specifications, we now calculate ion-displacement through the filter for an ion coming in at angle θ to the x-axis with some initial displacement z_0 in the z-axis and initial velocity $\mathbf{v}(t=0) = |\mathbf{v}|\cos\theta\hat{i} + |\mathbf{v}|\sin\theta\hat{j}$, with the electric field in direction $\hat{j}$ and magnetic field in direction $\hat{k}$, illustrated in figure 7. Using $F = ma$, where $F = q(\mathbf{E} + v \times \mathbf{B})$ is the Lorentz Force we have

$$m(\ddot{x}(t)\hat{i} + \ddot{z}(t)\hat{j}) = q(E\hat{j} + (v_x(t)\hat{i} + v_z(t)\hat{j}) \times B\hat{k})$$

giving two coupled second-order differential equations in accelerations $\ddot{x}(t)$ and $\ddot{z}(t)$

$$m\ddot{x}(t) = Bq\dot{z}(t) \tag{6}$$

$$m\ddot{z}(t) = qE - Bq\dot{x}(t) \tag{7}$$

Solutions $x(t)$ and $z(t)$ can be obtained by uncoupling equations 6 and 7. Equation 6 can be differentiated with respect to t to obtain an expression for $\ddot{z}(t)$, which can be substituted into equation 7 to obtain a non-homogeneous third-order differential equation in $x(t)$

$$\frac{m^2}{Bq}\dddot{x}(t) + Bq\dot{x}(t) = qE \tag{8}$$

Similarly, we can differentiate equation 7 with respect to t to obtain an expression in $\ddot{x}(t)$, substituting into equation 6 to obtain a homogenous third order differential equation in $z(t)$, given by

$$\frac{m^2}{Bq}\dddot{z}(t) + Bq\dot{z}(t) = 0 \tag{9}$$

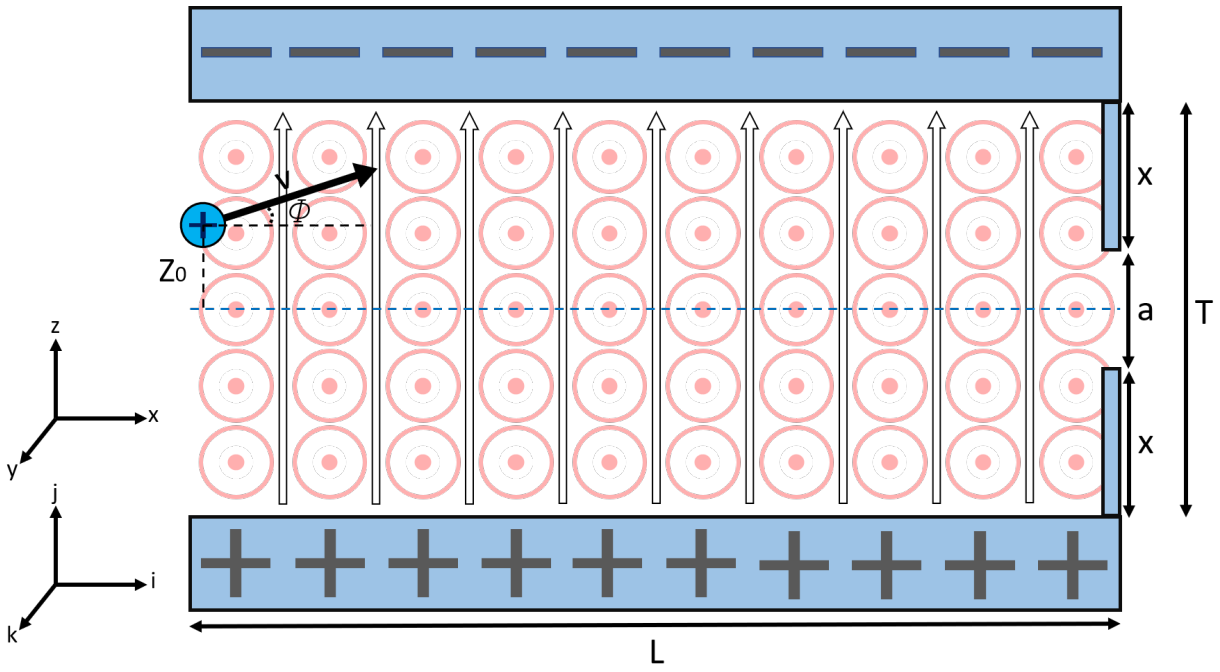

Figure 7: Schematic illustration of a Wien filter with aperture size a and electrode separation T where an arbitrary positive ion enters the filter with velocity v, angle θ and initial displacement z_0

Equation 8 can be solved via substitution. Let $w(t) = \dot{x}(t)$, giving a second order differential equation in $w(t)$

$$\ddot{w}(t) + \frac{q^2B^2}{m^2}w(t) - \frac{q^2BE}{m^2} = 0 \tag{10}$$

The homogeneous solution to which is

$$w(t) = A_1 \cos\frac{Bqt}{m} + A_2 \sin\frac{Bqt}{m} \tag{11}$$

and the particular solution is

$$w(t) = \frac{E}{B} \tag{12}$$

giving the full solution

$$w(t) = A_1 \cos\frac{Bqt}{m} + A_2 \sin\frac{Bqt}{m} + \frac{E}{B} \tag{13}$$

Substituting $w(t) = \dot{x}(t)$ and letting $c_1 = \frac{-A_2 m}{Bq}$ and $c_2 = \frac{A_1 m}{Bq}$ we obtain an expression for the velocity $\dot{x}(t)$

$$\dot{x}(t) = c_2\frac{Bq}{m}\cos\frac{Bqt}{m} - c_1\frac{Bq}{m}\sin\frac{Bqt}{m} + \frac{E}{B} \tag{14}$$

Equation 14 can be differentiated to obtain an expression for $\ddot{x}(t)$ and substituted into equation 6 to obtain an expression for the velocity $\dot{z}(t)$

$$\dot{z}(t) = -c_1 \frac{Bq}{m} \cos \frac{Bqt}{m} - c_2 \frac{Bq}{m} \sin \frac{Bqt}{m} \tag{15}$$

Integrating equations 14 and 15 we obtain solutions for $x(t)$ and $z(t)$

$$x(t) = c_1 \cos \frac{Bqt}{m} + c_2 \sin \frac{Bqt}{m} + \frac{E}{B}t + c_3 \tag{16}$$

$$z(t) = -c_1 \sin \frac{Bqt}{m} + c_2 \cos \frac{Bqt}{m} + c_4 \tag{17}$$

Initial conditions for the displacements $x(t)$, $z(t)$ and velocities $\dot{x}(t)$, $\dot{z}(t)$ for a beam of particles coming in arbitrary angle θ and with arbitrary initial z-displacement $= z_0$ at time $t = 0$ are

$$x(t = 0) = 0$$
$$z(t = 0) = z_0$$
$$\dot{x}(t = 0) = |\mathbf{v}| \cos \theta$$
$$\dot{z}(t = 0) = |\mathbf{v}| \sin \theta$$

Applying these initial conditions to find values of c_1, c_2, c_3 and c_4 we obtain full solutions to $x(t)$, $z(t)$, $\dot{x}(t)$ and $\dot{z}(t)$

$$x(t) = -\frac{m|v|}{Bq} \sin \theta \cos \frac{Bqt}{m} + \frac{m}{Bq}(|v| \cos \theta - \frac{E}{B}) \sin \frac{Bqt}{m} + \frac{m|v|}{Bq} \sin \theta + \frac{E}{B}t \tag{18}$$

$$z(t) = \frac{m|v|}{Bq} \sin \theta \sin \frac{Bqt}{m} + \frac{m}{Bq}(|v| \cos \theta - \frac{E}{B})(\cos \frac{Bqt}{m} - 1) + z_0 \tag{19}$$

$$\dot{x}(t) = |v| \cos (\theta - \frac{Bqt}{m}) + \frac{E}{B}(1 - \cos \frac{Bqt}{m}) \tag{20}$$

$$\dot{z}(t) = |v| \sin (\theta - \frac{Bqt}{m}) + \frac{E}{B} \sin \frac{Bqt}{m} \tag{21}$$

where equations 18 and 19 are the displacements in the x and z directions and equations 20 and 21 are the velocities in the x and z directions, respectively.

5.1 MATLAB

We now use MATLAB to evaluate expressions 18 and 19 for a prototypical room temperature ionic liquid EMI $-$ BF_4 in positive emission and provide an estimate for filter length required to successfully deflect and trap unwanted ions. Conventional Wien filters utilise aperture sizes of $a = 0.5 - 1.5$ mm and magnetic flux densities of $B = 200 - 500$ mT [22]. Here we define

$$\begin{aligned} B &= 500 \text{ mT} \\ q &= 1.6 \times 10^{-19} \text{ C} \\ \theta &= 0 \\ z_0 &= 1 \times 10^{-4} \text{ m} \\ a &= 1 \times 10^{-3} \text{ m} \\ V_0 &= 1000 \text{ V} \end{aligned}$$

where q is the charge of an electron, θ is the initial angle the ion approaches with, normal to the filter, z_0 is initial ion displacement perpendicular to ion motion and V_0 is the acceleration voltage applied at the emission site. We aim to isolate DE monomers EMI^+, with mass $m_A = 111$ atomic mass units (amu) and velocity $v_{DE,0} = 41,696$ ms^{-1}, given by equation 1 and parameters defined above, and trap all other species. DE monomers leave the Wien filter undeflected when the Lorentz force acting on them is zero. This occurs when the velocity of the incoming ions, here $v_{DE,0}$, is equal to the ratio E/B. Having defined $B = 500$ mT and $v_{DE,0}$ given by equation 1, we have that $E = 20,848$ Vm^{-1}.

We can equate expression 19 with some minimum displacement S_{min}, required to trap unwanted particles, and then solve for t. This time t can then be substituted into equation 18 to find the displacement in the x-direction i.e. the length of the filter. Practical ILIS beams have a parabolic distribution of particles, with a large number of particles concentrated in the centre of the beam. Therefore, a large number of particles approach the filter with small initial angle θ and displacement z_0. In order to deflect and trap such ions, the filter needs to cause a displacement of $\frac{a}{2}$, where a is aperture size. Therefore, we define $S_{min} = \frac{a}{2}$.

We can evaluate expressions 18 and 19 for various ionic species to obtain estimates of

filter parameters needed to trap or isolate the species. Here, we demonstrate that the model does indeed provide reasonable estimates by evaluating expressions 18 and 19 for dimer ions $(\mathrm{EMI}-\mathrm{BF_4})\mathrm{EMI}^+$, with mass $m_{\mathrm{k=1}} = 309$ amu and velocity $v_{\mathrm{DE,k=1}} = 24,973\ \mathrm{ms}^{-1}$ given by equation 2 and parameters defined earlier in the section. In order to cause a z-displacement of at least S_{min}, evaluating equation 19 we find that the dimer needs to spend 8.31×10^{-7} seconds inside the filter. Using equation 18 this equates to an $x-$displacement of 2.08 cm. This is the minimum filter length necessary to cause a z-displacement S_{min} and trap dimers present in an $\mathrm{EMI}-\mathrm{BF_4}$ ILIS beam. This is in-line with practical filters where the distance between the extractor electrode and focusing lens is ~ 3 cm.

Now that we have an approximate filter length $L = 2.08$ cm that will adequately remove dimers $(\mathrm{EMI}-\mathrm{BF_4})\mathrm{EMI}^+$, we proceed by calculating the displacement of AR monomers EMI^+, with mass m_{A} and velocity v_{b}, given by equation 5, as a function of $\alpha = \frac{V_{\mathrm{b}}}{V_0}$, to judge the efficacy of the filter in trapping unwanted AR monomers. Figure 8 compares the ion displacements caused by filters, with aperture size $a = 1$ mm, with two different lengths: 2.08 cm (blue line) and 3 cm (red line). The shorter filter shows that AR monomers completely escape the filter if the fragmentation occurs after $\alpha = 0.55$. The longer filter, at 3 cm, however shows that AR monomers escape after $\alpha = 0.736$. A longer filter will trap a greater number of AR monomers as time spent in the filter, hence z-displacement, is greater. Therefore in this report we design a filter with a length of 3 cm. At the time of writing it is unclear whether fragmentation in the AR occurs uniformly across the electric potential range and so the benefit of a longer filter is questionable. Further investigation of the nature of fragmentation in the AR is needed to determine the effectiveness of a longer filter.

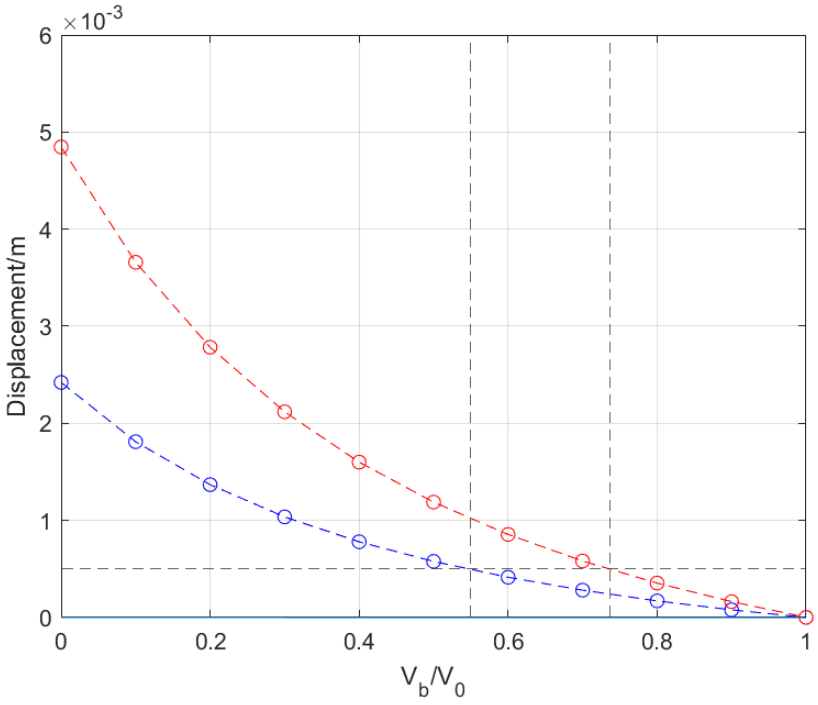

Figure 8: Scatter plot with a red dotted line of best fit showing z-displacement (red circles) inside filter for AR-fragmented ions from $\alpha = 0$ to $\alpha = 1$ for a filter length of 3 cm and blue dotted line of best fit (blue circles) showing z-displacement with a filter length of 2.08 cm. Note that $\alpha = \frac{V_b}{V_0}$.

6 COMSOL

The mathematical model, computed in MATLAB, described so far is excellent for prototyping filter parameters for a given ILIS and evaluating resulting ion displacements. However, the model, incorrectly, assumes uniform electric and magnetic fields, resulting in potentially erroneous ion-displacement figures. To obtain ion displacements that are more accurate, COMSOL Multiphysics is being used to simulate the Wien filter.

Here, we use COMSOL to numerically solve for and computationally approximate electro- and magneto-static fields and ion trajectories through a Wien filter, using the finite element method (FEM). FEM is a numerical method for solving systems of partial differential equations. FEM divides a large system into smaller parts that are called finite elements. This is achieved via discretization, implemented e.g. via the construction of a mesh of a (computer

aided design) CAD object. The method approximates the values of the unknown functions within the finite elements. The method then uses calculus of variations to approximate a solution by minimizing an associated error function. A more detailed discussion of the mesh used and errors associated is in section 6.4.

Here we solve our model using the AC/DC module, which allows simulation of electro- and magneto-static systems, and (charged particle traing) CPT module which allows calculation of charged particle path-tracing through electromagnetic fields.

6.1 Filter Design

A Wien filter needs to generate uniform, perpendicular electric and magnetic fields in order to correctly deflect charged species. We use electrostatic deflectors and permanent magnets to produce the desired electric and magnetic fields, respectively.

Typically, velocity selectors will use an iron yoke to hold the magnets and electrostatic deflectors in place [23] as well as to promote more uniform magnetic fields and to reduce electromagnetic fields leaking outside the filter which can cause premature ion displacements. Figure 9 illustrates a 3-dimensional isometric projection of the proposed design for a Wien filter with figure 10 showing a 2-dimensional orthographic projection for better clarity.

The filter features two permanent magnets, magnetised and placed along the y-axis and two T-shaped electrostatic deflectors placed along the z-axis that generate an electric field also along the z-axis. Electric and magnetic field directions are in the -z and y directions, respectively while the ion beam travels in the +x direction. The yoke can be manufactured either out of a single block or two separate blocks of soft iron, with a higher purity resulting in a higher relative permeability and therefore more uniform field lines, with space to hold the magnets in place. The yoke prevents movement of the magnets in the y-direction via the cutout lips. To prevent movement of the magnets in the x-direction aperture plates, with holes (or apertures) in them for beam travel, can be placed on either end of the yoke and screwed in place. This allows for both quick removal and replacement of the permanent magnets as well as aperture plates with different sized apertures. Here, we simulate a Wien filter with an entry aperture of 0.2 cm and an exit aperture of 0.1 cm, which are typical numbers [22]. The electrostatic deflectors can be held in place via stiff insulated wires that

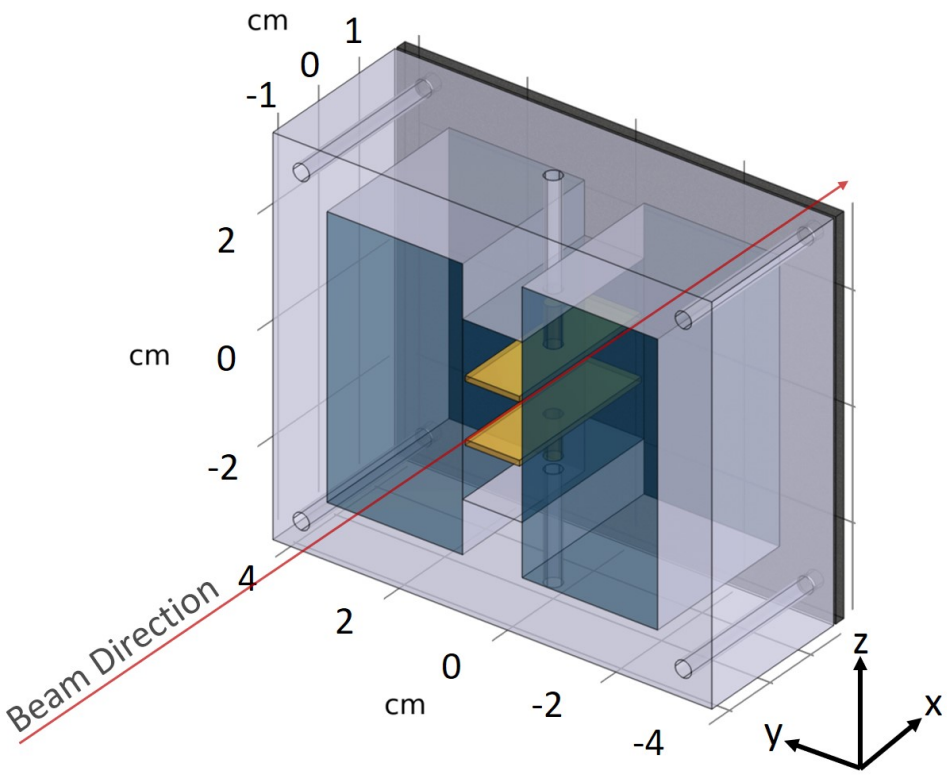

Figure 9: Translucent illustration of the proposed Wien filter, with the magnets coloured blue, electrodes gold, iron yoke grey, aperture plates black and beam direction shown by the red arrow. Note that the entry aperture plate has been omitted here for better clarity, while the black exit aperture is still visible behind the yoke.

fit in to the T-shape. The wires are passed through the yoke via holes at the top and bottom of the yoke, visible in figure 10 (b). Figures 10 (b) and (c) also show holes for the stiff electrode wire and screws, respectively.

Permanent magnets are a preferred choice here as the magnets can simply be removed or swapped out without risk of residual fields interfering. There are five types of permanent magnets: alnico, samarium cobalt, ferrite (also known as ceramic), flexible rubber and Neodymium Iron Boron (or simply Neodymium) available [24]. Neodymium magnets offer the highest magnetic strength but have weaker corrosion resistance than other magnet types. However, corrosion-resistant coating can always be applied to the magnet surface and so here we use N52 sintered Neodymium magnets, which is the strongest grade of magnets commercially available.

The aperture plates and electrodes can be manufactured out of stainless steels, which are corrosion resistant alloys of iron, chromium, nickel and other metals, available in five groups: martensitic, austenitic, ferritic, duplex and precipitation-hardened steels, each with varying ratios of substituent elements, leading to a large variety of material properties [25].

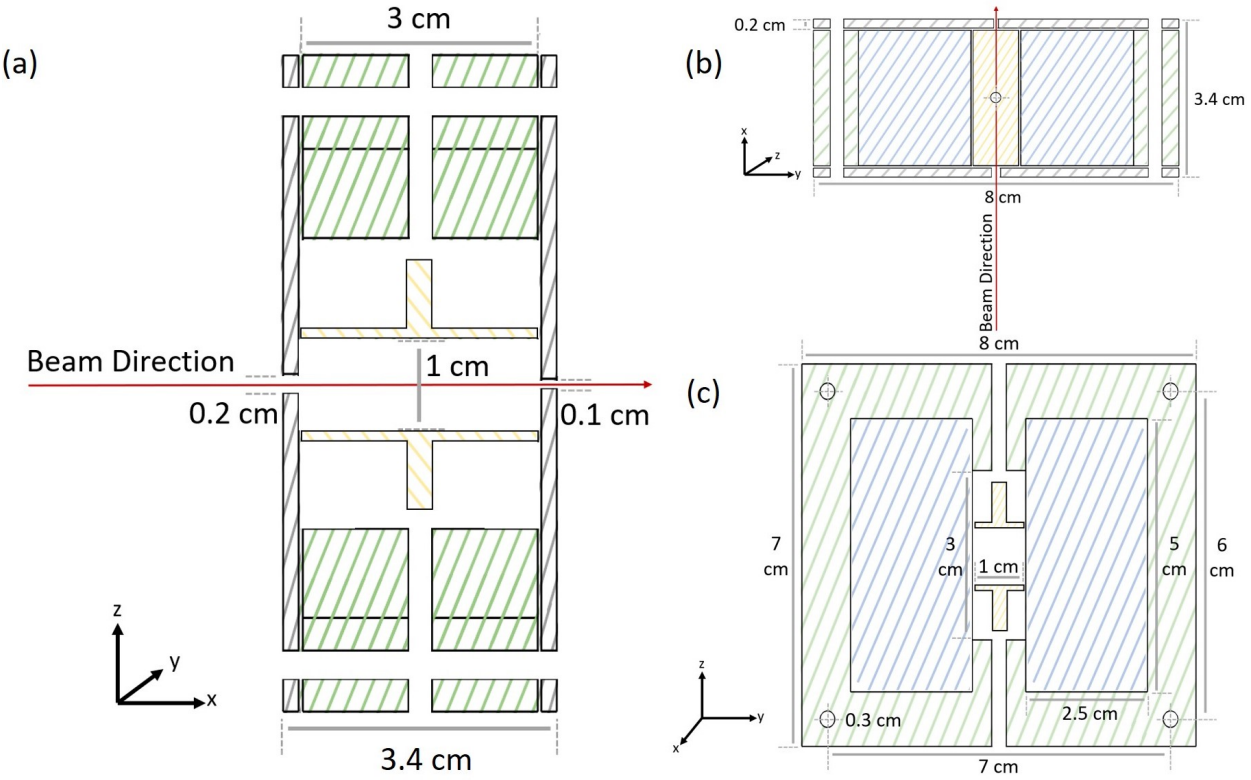

Figure 10: Schematic cross-sections in the (a) xz, (b) xy and (c) yz planes with the magnets shaded blue, electrodes gold, yoke green and aperture plates grey, and beam direction in the x-axis shown via the red arrow. Note that the cross-sections are cut through the centre of the filter in each plane.

For our purposes, the aperture plates need to have a high relative permeability to prevent leakage of the magnetic fields and avoid premature changes to ion trajectory as well as have good corrosion resistance. The electrodes, likewise, need to have good corrosion resistance however need a low relative permeability so as not to perturb the surrounding magnetic fields. Therefore, we suggest ferritic stainless steels for the aperture plates and martensitic stainless steels for the electrodes and use these in the COMSOL simulation.

The filter has a length (x-direction) of 3.4 cm. The effective filter length an ion beam

experiences is 3 cm with an additional 0.2 cm being added at either end from the aperture plates leading to a total filter length of 3.4 cm. It has a width (y-direction) of 8 cm and height (z-direction) of 7 cm. The electrostatic deflectors have length 3 cm, width 1 cm and thickness 0.1 cm with the T adding an additional 0.8 cm. The magnets have length 3 cm, width 2.5 cm and height 5 cm. The effective cross-sectional area the ion beam can travel through in the filter is 1 cm $\times$ 1 cm, for a length of 3 cm.

The COMSOL model is run with the filter inside a box of perfect vacuum. The magnets, yoke and aperture plates are all electrically grounded to prevent leakage of the electric field. A magnetic flux density of $B = 500$ mT and an electric field strength of $E = 20848$ Vm^{-1}, values from section 5, are desired at the centre of the filter to allow DE monomers EMI^+ with velocity $v = \frac{E}{B}$, given by equation 1, to escape the filter undeflected.

6.2 Field Quality

COMSOL calculates the electric fields using Gauss' Law of electrostatics given by equation 22, which relates the divergence of an electric displacement field $\mathbf{D}$ to the volume charge density ρ

$$\nabla \cdot \mathbf{D} = \rho \tag{22}$$

where $\mathbf{D}$ is a vector sum of the applied Electric field and induced polarisation density and is given by

$$\mathbf{D} = \epsilon_0 \mathbf{E} + \mathbf{P} \tag{23}$$

Additionally, Faraday's law of electrostatics enforces that an Electric field be irrotational and therefore satisfy

$$\nabla \times \mathbf{E} = 0 \tag{24}$$

$$\mathbf{E} = -\nabla\ V \tag{25}$$

In free space, Gauss' magnetic law forbids the existence of monopoles and enforces

$$\nabla \cdot \mathbf{B} = 0 \tag{26}$$

where $\mathbf{B}$ is the magnetic flux density e.g. from a permanent magnet. In the case of no free currents, the magnetic field intensity $\mathbf{H}$ generated by a permanent magnet is irrotational

and characterised by

$$\mathbf{H} = \frac{\mathbf{B}}{\mu} - \mathbf{M}\nabla \cdot \mathbf{H} = 0 \tag{27}$$

$$\mathbf{H} = -\nabla\ V_{\mathrm{m}} \tag{28}$$

COMSOL uses equations 22 - 28 to calculate the electromagnetic fields used. Figure 11 shows the electric and magnetic fields obtained from the COMSOL model without the use of an iron yoke. Figure 12 shows the same fields with an iron yoke.

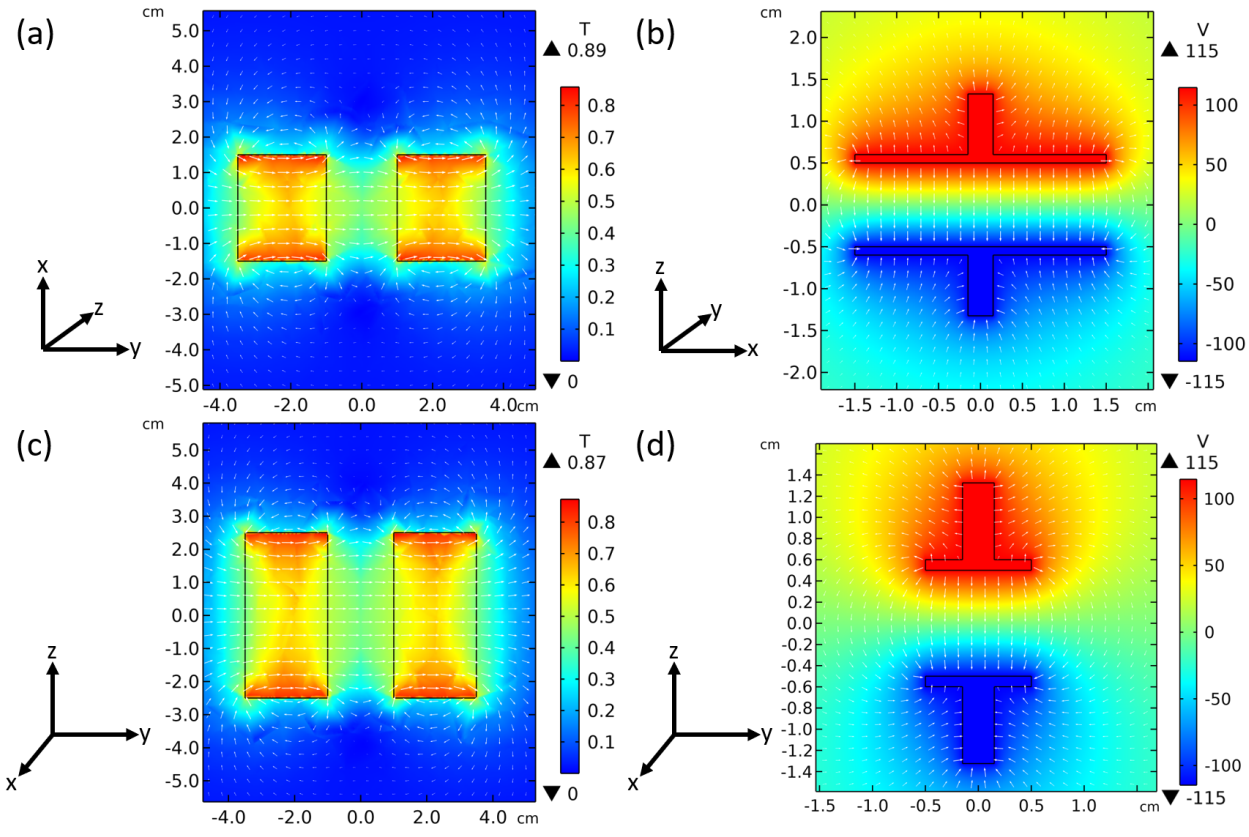

Figure 11: COMSOL field diagrams showing electric potential between two electrostatic deflectors in the (b) zx and (d) zx planes, and magnetic intensity between two 0.834 mT NdFeB magnets in the (a) xy and (c) zy planes. Fields are visualised via the colour and strength and direction shown via logarithmically scaling arrows. Note the absence of a yoke here.

The fields are calculated using a stationary state time-independent study. For the filter to be effective, a field strength of 500 mT is required at the centre of the filter, however,

magnetic fields can show a rapid decline spatially. The model was found to produce a magnetic field strength of 500 mT at the centre if magnets with field strengths of 834 mT were used. It was found, via trial and error, that a potential difference of 229 V between the electrostatic deflectors produced the best results and caused minimal z-displacement for DE monomers.

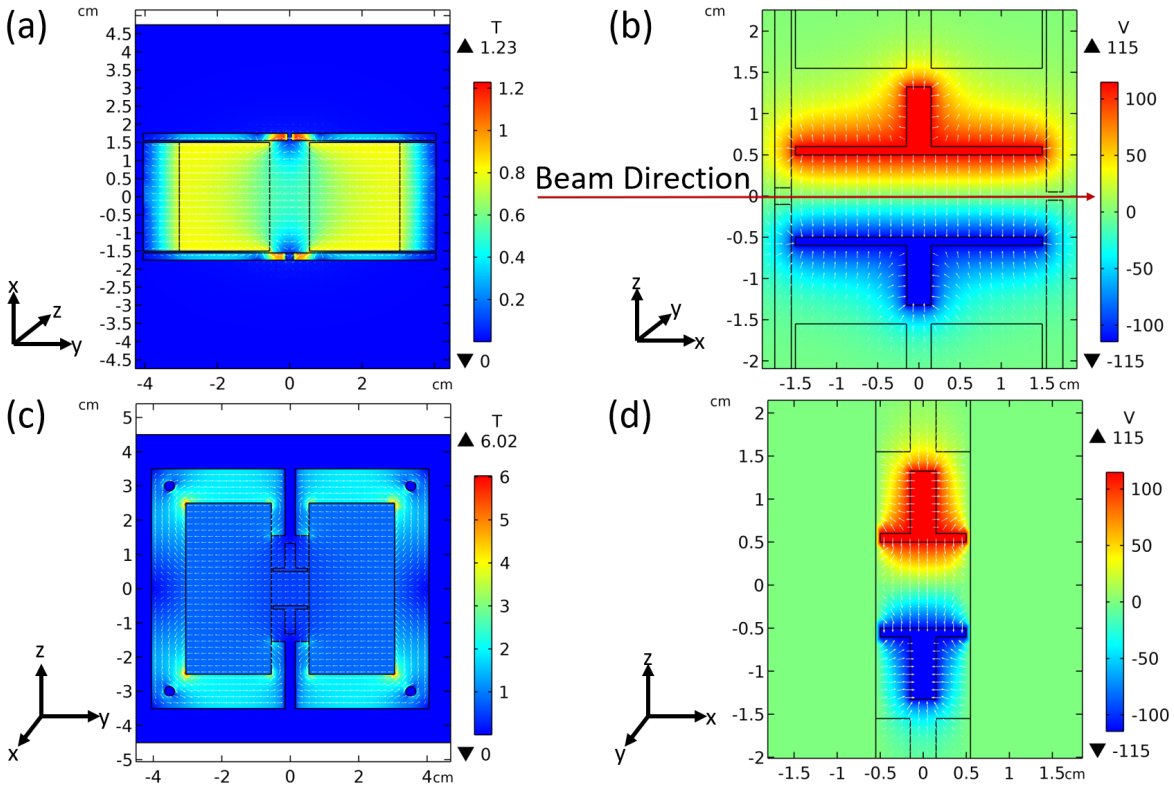

Figure 12: COMSOL field diagrams showing electric potential between two electrostatic deflectors in the (b) zx and (d) zx planes, and magnetic intensity between two 0.834 mT NdFeB magnets in the (a) xy and (c) zy planes. Fields are visualised via the colour and strength and direction shown via logarithmically scaling arrows. Note the presence of a yoke here.

It is clear from figures 11 and 12 that in addition to holding the magnets and electrostatic deflectors in place, the yoke also helps to create more uniform electromagnetic fields. COMSOL also shows some artefacts in the magnetic flux density, particularly at the corners of the magnets and yoke. This is believed to be caused by the sharpness of the edges and can be relieved by using a finer mesh at the edges. However, we are only interested in

the field strength in the center of the filter, which shows no such artefacts and therefore it is unnecessary to spend the extra computational resources to alleviate these edge-artefacts which do not impact filter performance. Further discussion about the mesh options used is outlined in section 6.4.

6.3 Beam Simulation

Filter performance is evaluated via the CPT module, which allows for a time-varying study of particle trajectories. The force on a moving charged particle, given by the Lorentz force

$$F = q(\mathbf{E} + v \times \mathbf{B}) \tag{29}$$

is used by COMSOL to evaluate particle displacements through the electromagnetic fields.

The ion beam from an ILIS emitting in the PIR has a conical profile, with a parabolic distribution of particles. Practical beams are composed of a mixture of monomers, oligomers, neutrals and various products of fragmentation occuring both in the AR and FFR, each species with their own energy and spatial distributions. For our purposes it is unnecessary to model such a "mixed particle" ion beam as filter performance can be better understood if beams of a single ion species are studied one at a time. Therefore in this project we investigate beams composed entirely of a single ionic species. We first investigate the ion displacement experienced by ions emitted in a single-particle fashion normal to the filter, i.e. with angle $\theta = 0$, and initial z-displacement $z_0 = 0$. The results are outlined in section 6.3.1. We then investigate how a conical beam, composed of a single species of ions, with a parabolic distribution of several particles, behaves in the filter. This is repeated for beams consisting of DE monomers, DE dimers, AR monomers and FFR monomers. The results are outlined in section 6.3.2. Filter parameters outlined in section 6.1 are used with $\mathrm{EMI-BF_4}$ as the ILIS, producing monomers $\mathrm{EMI^+}$ and dimers $(\mathrm{EMI-BF_4})\mathrm{EMI^+}$. Note that we restrict our study to monomers and dimers only and consider dimer fragmentation to strictly result in monomers and neutrals, as highlighted in section 5. Additionally, the high velocity of ions and short filter length reduce the impact of particle-particle interactions and so we ignore these interactions entirely in the following analyses.

6.3.1 Single Particle Emission

Figure 13 shows ion displacements of AR monomers released in a single-particle fashion normal to the filter, with $\theta = 0$ and $z_0 = 0$, obtained from COMSOL (purple dotted line) and overlayed onto the results of our mathematical model (red solid line) in section 5 for comparison. Displacement figures show excellent agreement with the mathematical model. The model predicted that dimers that fragment after $\alpha = \frac{V_b}{V_0} = 0.736$, where V_b is the electric potential at which fragmentation occurs in the AR and V_0 is the acceleration voltage at the emission site, will have a z-displacement less than $S_{min} = 0.5$ mm, defined in section 5.1, and will therefore escape the filter. The COMSOL model is in close agreement with $\alpha = 0.724$.

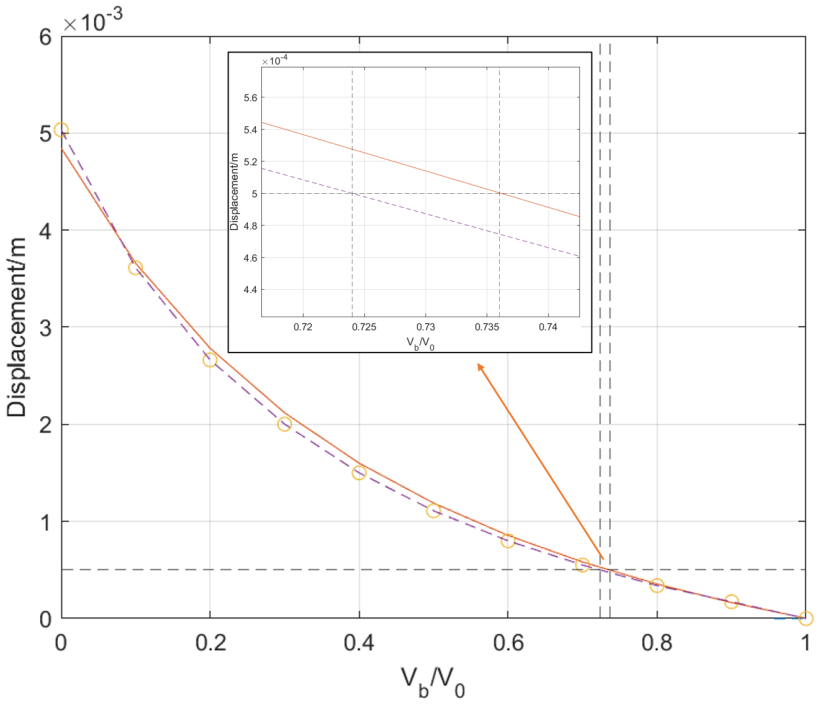

Figure 13: Scatter plot with a red solid line showing z-displacement inside filter for AR-fragmented monomers EMI^+ from $\alpha = 0$ to $\alpha = 1$ from our computational model and purple dotted line of best fit (yellow circles) showing z-displacement obtained from COMSOL model. A part of the plot is shown enlarged where it can be seen that COMSOL predicts dimers that fragment after $\alpha = 0.724$ will escape the filter while the mathematical model predicts a value of $\alpha = 0.736$.

Note that AR monomers resulting from fragmentation at $\alpha = 0$ have a velocity $v_{\mathrm{DE,k=1}}$

(equation 2) and mass m_A and are by definition FFR monomers with the same z-displacement. The filter is excellent at removing these. Conversely, AR monomers resulting from fragmentation at $\alpha = 1$ have a velocity $v_{DE,0}$ (equation 1) and mass m_A and are by definition DE monomers. This is evident in figures [13 - 16] where particles that fragment at $\alpha = 1$ experience 0 z-displacement and those that fragment at $\alpha = 0$ experience the maximum z-displacement. A separate study was carried out to evaluate the z-displacement of DE dimers. The mathematical model predicted a z-displacement of 1.9×10^{-3} m for a filter length of 3 cm. The COMSOL model is in close agreement with a z-displacement of 1.7×10^{-3} m.

6.3.2 Conical Beam of Ions

Here we use COMSOL to generate a conical beam of particles normal to the filter with a symmetric parabolic distribution. The conical beam travels at a maximum velocity v, with the transverse component, perpendicular to beam travel, given by $\sin(\theta)$ and longitudinal component, parallel to beam travel, given by $\cos(\theta)$, where $\theta = 0.05$ rad is the cone angle of emission such that if the beam were emitted from a point source 2 cm upstream from the entry aperture with a conical profile, it would arrive at the entry aperture with a diameter equal to that of the entry aperture, which in our study is $a = 1$ mm. Beams of 50,000 incident particles were used, released instantaneously at time t = 0. The study resulted in a maximum computation time of 1 minute 15 seconds.

Figure 14 shows the percentage of AR monomers, released in a conical fashion, that were found to escape the filter in a COMSOL study.

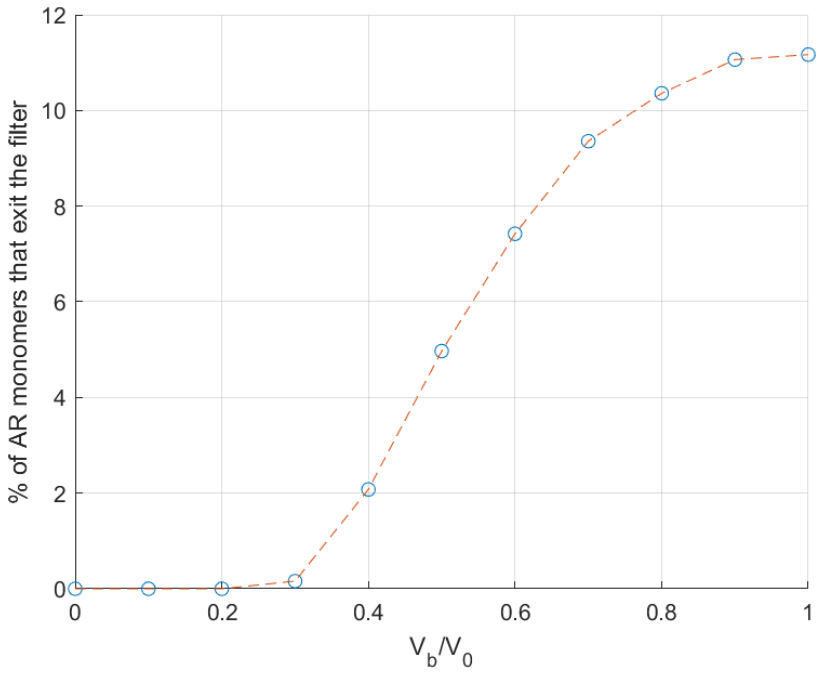

Figure 14: Percentage of AR monomers EMI^+ that are found to escape the filter, for 50,000 entry ions, where $\alpha = \frac{V_b}{V}$. Data points obtained from COMSOL.

The number of particles that escape the filter are counted by a particle counter placed 2 cm downstream from the exit aperture. The percentage of escaped ions is then given by $\frac{\text{escaped ions}}{\text{total incident ions = 50,000}} \times 100$. Due to the conical nature of the beam, significant ion escape can be observed after $\alpha = 0.3$, much earlier than observed in figure 13. Even with dimers fragmenting at $\alpha = 1$ i.e. when the resultant AR monomer behaves like a DE monomer, a maximum of only 11.2 % of particles escape the filter. This is a significant but expected loss in particle numbers from a conical beam. Figure 15 visualises beam trajectories inside the filter for AR and FFR monomers, in the xz plane. It is clear that as α increases, ion displacements caused by the filter decrease and a greater portion of the beam escapes the filter. This is problematic for applications, like FIB, where control over the emitted ionic species is desirable. Note the similarity between figures 15(a) and (l) that occurs because AR monomers that result from fragmentation of dimers at $\alpha = 0$ carry the same velocity as the dimers $v_{\mathrm{DE,k=1}}$ and mass $\mathrm{m_A}$ and so are, by definition, FFR monomers.

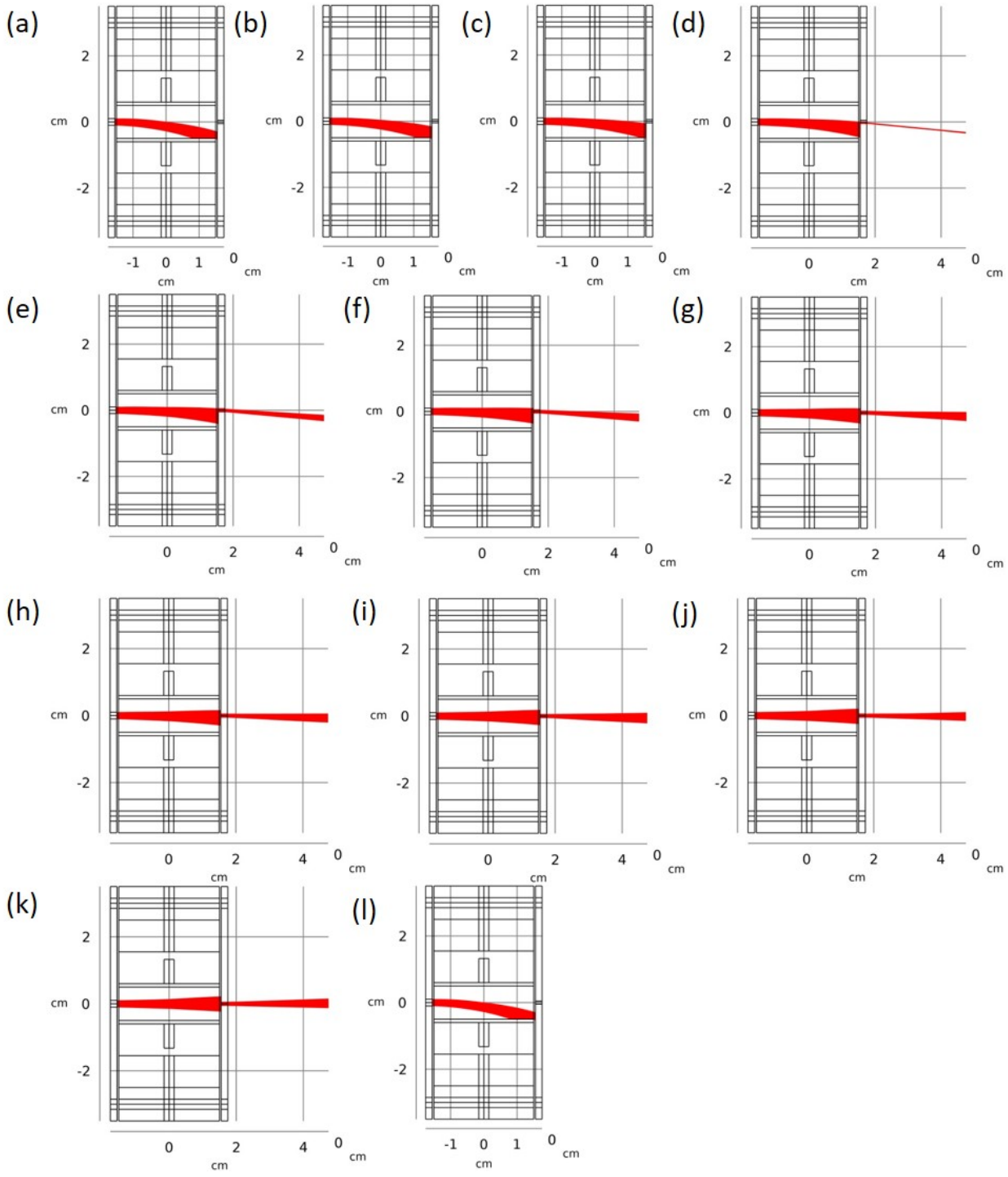

Figure 15: Ion trajectories for AR monomers EMI^+ with $\alpha = 0$ increasing to $\alpha = 1$ from diagrams (a) to (k). Diagram (l) shows ion trajectory for FFR monomers EMI^+.

Figure 16 visualises beam trajectories inside the filter for DE monomers and DE dimers,

in the xz plane, with ion distributions shown via Poincaré maps placed at the entry aperture, exit aperture, and 2 cm downstream from the exit aperture.

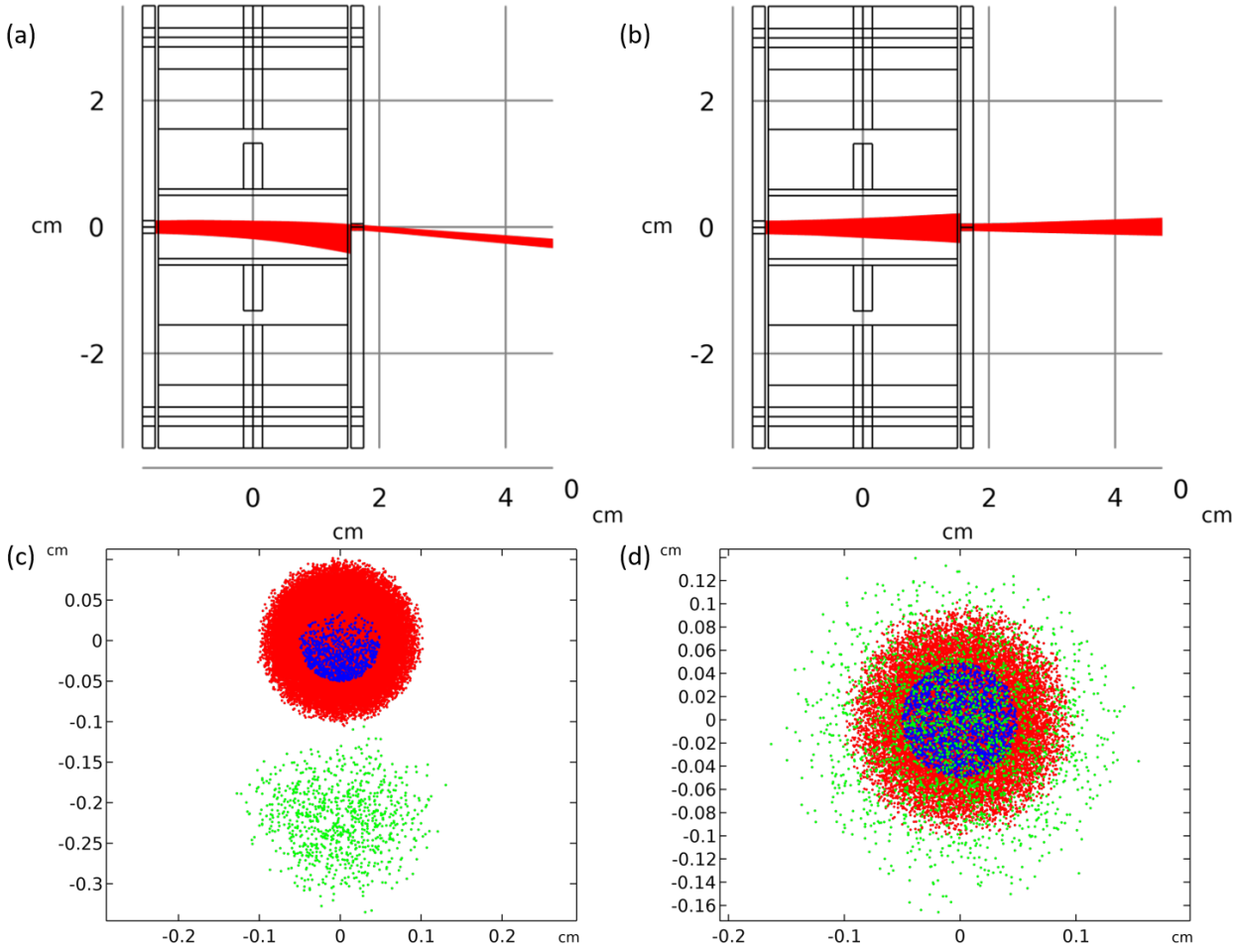

Figure 16: Ion trajectory for (a) DE dimer beam, (b) DE monomer beam and Poincaré maps of (c) DE dimers and (d) DE monomers with the red showing ions at the entrance aperture, blue at the exit aperture and green 2 cm downstream from the exit aperture. Each dot represents a single ion.

It is observed that out of 50,000 incident DE dimers, 1.75 % escape the filter. Figure 16(c) shows the escaped DE dimer beam is highly deflected. Conversely, 11.2 % of DE monomers escape the filter, with minimal deflection. Note the similarity between figures 15(k) and 16(b) that occurs because AR monomers that result from fragmentation at $\alpha = 1$ have undergone full acceleration in the AR as a monomer and so are, by definition, DE monomers.

6.4 Errors and Mesh Refinement

COMSOL uses the FEM to numerically solve systems of differential equations. The software uses an iterative solving method. It subdivides a CAD model into a surface mesh and attempts to solve the model at each mesh point for a very coarse mesh, it then subdivides and makes the mesh finer and attempts to solve the model once again. This is repeatedly done until a mesh density set by the user is achieved. It is important that the solution arrived at by COMSOL is mesh-convergent. This is achieved when a global/local mesh refinement does not significantly change the results [26]. For efficient modeling the goal is to create a mesh that just fulfills mesh convergence but is not finer than necessary in order to keep computational expense as low as possible. For particularly complicated models, custom mesh densities can be defined where the element size is very fine in particular areas of interest and coarse in other areas. For the purposes of this study, COMSOL uses mesh data to calculate electric and magnetic field strengths. It was found, by trial and error, that a Physics-controlled "fine" mesh applied to the entire model was sufficient to produce reasonably detailed electromagnetic fields while keeping computation times low, achieving convergence within a few iterations. Computation times for stationary state studies used for electromagnetic field calculations was a maximum of 56 seconds, which was considered reasonable.

7 Summary and Further Work

Herein we have proposed and evaluated a design for a Wien filter to be used in ILIS columns. A mathematical model to calculate ion trajectories through a Wien filter has been developed and further analysis has been carried out using COMSOL Multiphysics where ions from a $EMI-BF_4$ source have been studied. The Wien filter in this study was found to completely remove FFR monomers, and AR monomers that result from fragmentation before $\alpha = \frac{V_b}{V_0} = 0.3$. An increase in escape percentage is seen for AR monomers that result from fragmentation after $\alpha = 0.3$ with a peak escape percentage of 11.2 % for $\alpha = 1$. A small percentage, 1.75 % of DE dimers are observed to escape the filter.

Analysis was kept confined to the study of DE monomers, DE dimers, AR monomers

and FFR monomers with a key assumption that dimer fragmentation always results in a monomer and a neutral. This is a limitation of the current study as practical beams will be composed of higher order oligomers that are also subject to fragmentation in the AR and FFR, resulting in a large variety of smaller oligomers and neutrals. Further limitations are imposed by the tools provided by COMSOL Multiphysics to simulate particle beams. The software does not readily simulate particle beams with custom spatial, energetic and species distributions. The studies conducted here assume that all ionic species will be uniformly distributed in a parabolic fashion, which is a simplification. However, COMSOL does provide a Python scripting interface that can be used to construct more complex custom models, which was not used in the current study. Further work can be done by more accurately simulating the particle beam leading to better, more suited filter parameters. Further deliberation is also required on material choices for the Wien filter, ensuring good corrosion resistance and long lifetimes for electrode and magnet surfaces as well as minimising leakage of magnetic and electric fields outside the filter to reduce premature ion displacements. Additional studies testing other common ionic liquids like $EMIM-TFSI$, $EMIM-DCA$, $BMI-I$ and $EMI-FAP$ should provide further confidence in filter performance and further investigation of the nature of fragmentation in the AR is needed to determine the effectiveness of a longer filter, as mentioned in section 5.1. Successful implementation of Wien filters in ILIS columns will afford great control over the type of ionic species used and lead to material treatment characteristics that far surpass currently available technologies like LMIS.

References

[1] sigmaaldrich. (). Accessed: April 26, 2021, [Online]. Available: https://www.sigmaaldrich.com/catalog/product/sial/00768?lang=en&region=GB.

[2] C. Perez-Martinez and P. Lozano, "Ion field-evaporation from ionic liquids infusing carbon xerogel microtips," *Applied Physics Letters*, vol. 107, no. 4, p. 043 501, 2015.

[3] A. N. Zorzos and P. C. Lozano, "The use of ionic liquid ion sources in focused ion beam applications," *Journal of Vacuum Science & Technology B: Microelectronics and Nanometer Structures Processing, Measurement, and Phenomena*, vol. 26, no. 6, pp. 2097–2102, 2008.

[4] T. Xu, Z. Tao, and P. C. Lozano, "Etching of glass, silicon, and silicon dioxide using negative ionic liquid ion sources," *Journal of Vacuum Science & Technology B, Nanotechnology and Microelectronics: Materials, Processing, Measurement, and Phenomena*, vol. 36, no. 5, p. 052 601, 2018.

[5] C. E. Miller and P. C. Lozano, "Measurement of the dissociation rates of ion clusters in ionic liquid ion sources," *Applied Physics Letters*, vol. 116, no. 25, p. 254 101, 2020.

[6] C. S. Perez Martinez, "Engineering ionic liquid ion sources for ion beam applications," Ph.D. dissertation, Massachusetts Institute of Technology, 2016.

[7] I. Romero-Sanz, R. Bocanegra, J Fernandez De La Mora, and M Gamero-Castano, "Source of heavy molecular ions based on taylor cones of ionic liquids operating in the pure ion evaporation regime," *Journal of Applied Physics*, vol. 94, no. 5, pp. 3599–3605, 2003.

[8] P. Lozano and M. Martinez-Sanchez, "Ionic liquid ion sources: Characterization of externally wetted emitters," *Journal of colloid and interface science*, vol. 282, no. 2, pp. 415–421, 2005.

[9] P. Lozano and M. Martínez-Sánchez, "Ionic liquid ion sources: Suppression of electrochemical reactions using voltage alternation," *Journal of colloid and interface science*, vol. 280, no. 1, pp. 149–154, 2004.

[10] ——, "On the dynamic response of externally wetted ionic liquid ion sources," *Journal of Physics D: Applied Physics*, vol. 38, no. 14, p. 2371, 2005.

[11] N. Brikner and P. C. Lozano, "The role of upstream distal electrodes in mitigating electrochemical degradation of ionic liquid ion sources," *Applied Physics Letters*, vol. 101, no. 19, p. 193 504, 2012.

[12] L. Bischoff, P. Mazarov, L. Bruchhaus, and J. Gierak, "Liquid metal alloy ion sources—an alternative for focussed ion beam technology," *Applied Physics Reviews*, vol. 3, no. 2, p. 021 101, 2016.

[13] C. Perez-Martinez, S. Guilet, N. Gogneau, P. Jegou, J. Gierak, and P. Lozano, "Development of ion sources from ionic liquids for microfabrication," *Journal of Vacuum Science & Technology B, Nanotechnology and Microelectronics: Materials, Processing, Measurement, and Phenomena*, vol. 28, no. 3, pp. L25–L27, 2010.

[14] R. Yoshida, M. Hara, H. Oguchi, and H. Kuwano, "Micromachined multiple focused-ion-beam devices," *Journal of Vacuum Science & Technology B, Nanotechnology and Microelectronics: Materials, Processing, Measurement, and Phenomena*, vol. 34, no. 2, p. 022 001, 2016.

[15] Y. Yoshida and G. Saito, "Influence of structural variations in 1-alkyl-3-methylimidazolium cation and tetrahalogenoferrate (iii) anion on the physical properties of the paramagnetic ionic liquids," *Journal of Materials Chemistry*, vol. 16, no. 13, pp. 1254–1262, 2006.

[16] S Guilet, C Perez-Martinez, P Jegou, P Lozano, and J Gierak, "Ionic liquid ion sources for silicon reactive machining," *Microelectronic Engineering*, vol. 88, no. 8, pp. 1968–1971, 2011.

[17] D. G. Courtney, H. Q. Li, and P. Lozano, "Emission measurements from planar arrays of porous ionic liquid ion sources," *Journal of Physics D: Applied Physics*, vol. 45, no. 48, p. 485 203, 2012.

[18] M. Takeuchi, Y. Hoshide, T. Hamaguchi, H. Ryuto, and G. H. Takaoka, "Ion-beam deposition/etching using emim-n (cn) 2 ionic liquid ion source," *Transactions of the Materials Research Society of Japan*, vol. 40, no. 2, pp. 87–90, 2015.

[19] C. S. Perez-Martinez and P. C. Lozano, "Visualization of beams from ionic liquid ion sources for focused ion beam applications," *Journal of Vacuum Science & Technology B, Nanotechnology and Microelectronics: Materials, Processing, Measurement, and Phenomena*, vol. 30, no. 6, 06F601, 2012.

[20] T. P. Fedkiw and P. C. Lozano, "Development and characterization of an iodine field emission ion source for focused ion beam applications," *Journal of Vacuum Science & Technology B: Microelectronics and Nanometer Structures Processing, Measurement, and Phenomena*, vol. 27, no. 6, pp. 2648–2653, 2009.

[21] M. Takeuchi, Y. Hoshide, H. Ryuto, and G. H. Takaoka, "Sputtering of silicon and glass substrates with polyatomic molecular ion beams generated from ionic liquids," *Journal of Vacuum Science & Technology A: Vacuum, Surfaces, and Films*, vol. 34, no. 2, p. 02D108, 2016.

[22] D. GmbH. (). Accessed: 16-01-2021, [Online]. Available: `https://www.dreebit-ibt.com/shop/wien-filter.html`.

[23] M Salomaa and H. Enge, "Velocity selector for heavy-ion separation," *Nuclear Instruments and Methods*, vol. 145, no. 2, pp. 279–282, 1977.

[24] J. Coey, "Permanent magnets: Plugging the gap," *Scripta Materialia*, vol. 67, no. 6, pp. 524–529, 2012.

[25] L. Gardner, "Stability and design of stainless steel structures–review and outlook," *Thin-Walled Structures*, vol. 141, pp. 208–216, 2019.

[26] C. Fairclough. (). Accessed: 26-04-2021, [Online]. Available: `https://uk.comsol.com/blogs/efficiently-mesh-your-model-geometry-with-meshing-sequences/#:~:text=In%20COMSOL%20Multiphysics%2C%20meshing%20utilizes,Images%20of%20different%20element%20types.`.